# Stacked Antiaromaticity in the π-Congested Space Between the Aromatic Rings in the Anthracene Dimer

Tomohiko Nishiuchi,[a,c*] Yuta Makihara,[a] Ryohei Kishi,[b,c,d] Hiroyasu Sato,[e] and Takashi Kubo[a,c*]

[a] Department of Chemistry, Graduate School of Science, Osaka University, 1-1 Machikaneyama, Toyonaka, Osaka 560-0043, Japan.

[b] Department of Materials Engineering Science, Graduate School of Engineering Science, Osaka University, Toyonaka, Osaka 560-8531, Japan

[c] Innovative Catalysis Science Division, Institute for Open and Transdisciplinary Research Initiatives, (ICS-OTRI), Osaka University, Suita, Osaka 565-0871, Japan

[d] Research Center for Solar Energy Chemistry (RCSEC) and Center for Quantum Information and Quantum Biology (QIQB) Osaka University, Toyonaka, Osaka 560-8531, Japan

[e] Rigaku Corporation, 3-9-12 Matsubara, Akishima, Tokyo 196-8666, Japan

KEYWORDS. antiaromaticity, anthracene dimer, π-congestion, open-shell, hydrostatic pressure

E-mail: nishiuchit13@chem.sci.osaka-u.ac.jp

**Abstract**

Substance containing two π-congested aromatic systems are attractive targets in synthetic studies as well as efforts designed to explore the unique properties that originate from π-congestion. Since the time of the computational studies by Schleyer and Warner, the concept of stacked aromaticity created by the encounter of two antiaromatic rings has received much attention. A structure containing π-congestion between two antiaromatic norcorrole rings was prepared by Shinokubo *et. al*. In contrast, questions about what happens when two aromatic rings are closely stacked have remained unanswered. Specifically, the electronic consequences of stacking of two aromatic π-conjugated systems have not been fully evaluated. To the best of our knowledge, only one computational study has been performed by Herges, the results of which suggest that [2.2]paracyclophane, possessing short distance (<3.00 Å) between two aromatic ring planes, has a paratropic ring current between two the benzene rings. This observation is consistent with the conclusion that stacked antiaromaticity exists within the π-congested space between aromatic rings. Herein, we investigated the stacked antiaromaticity of highly π-congested anthracene dimers using anthracenophane, which possesses a short inter-plane carbon-carbon distance of *ca.* 2.80 Å. The absorption spectrum of this substance contains a weak broad band from 450 to 550 nm that is attributed from HOMO-LUMO transition. These properties exist in planar cyclooctatetraene derivatives that having 8π-electron antiaromaticity. The results of nucleus-independent chemical shift and anisotropy of the induced current density calculations indicate that relatively weak antiaromatic character exists between the central six-membered rings of the two anthracene moieties in anthracenophane. In addition, an attempt to enhance the stacked antiaromaticity of anthracenophane using pressure to enhance π-congestion was unsuccessful.

## 1. Introduction

[2.2]paracyclophane ([2.2]PC) is the typical π-congested molecule that two benzene rings are fixed by ethylene tether resulting in shorter carbon···carbon (C···C) distance from 3.09 to 2.83 Å between benzene rings than the sum of van der Waal's radii of carbon atoms (3.40 Å, Figure 1a).[1, 2] This short π-plane distance enable to exhibits a through-space π-conjugation and, therefore, multi-layered aromatic ring systems with the short π-π distance have been synthesized to elucidate the hole, electron, or exciton transporting properties through the congested aromatic planes.[3] Other type of cyclophanes composed of antiaromatic rings have been much attention because, in 2007, Schleyer and Warner computationally revealed the stacked two antiaromatic rings exhibits aromatic nature, that is, stacked aromaticity(Figure 1b).[4, 5] Recently, Shinokubo et. al., achieved the synthesis of stacked aromatic compound composed of two antiaromatic norcorrole rings (Figure 1c).[6] Although the stacked two antiaromatic ring systems have been so attractive target from experimentally and computationally, usual stacked two aromatic ring systems such as [2.2]PC have been less attention from the concept of aromaticity and antiaromaticity because no distinctive nature regarding the aromaticities had been predicted in aforementioned papers. On the other hand, in 2005, Herges et. al., reported a review on the anisotropy of the induced current density (ACID)[7] for a number of aromatic compounds. This review in chapter 4.3 notes that the [2.2]PC exhibits a paratropic ring current between two benzene rings via through-space and through-bond with ethylene tether, and concluded that [2.2]PC is not only destabilized by the high ring strain but also suffers from antiaromaticity (Figure 1d).[8] Thus, [2.2]PC is regarded as a stacked antiaromatic compound. However, to our best knowledge, no further computational and experimental studies for the stacked antiaromaticity have been investigated.

It is well known that anthracene undergoes [4+4] photodimerization, which is an allowed process according to the Woodward-Hoffmann rules and the transition state is classified as antiaromatic in the approaches proposed by Zimmerman and Dewar over 50 years ago.[9] A recent computational study revealed that the structure of excited state anthracene dimer (excimer), before undergoing [4+4]dimerization, exhibits Baird's aromaticity (Figure 2).[10,11] In addition, the [4+4] pericyclic reaction in ground state is a forbidden process Therefore, the ground state π-congested anthracene dimer is anticipated to possess stacked antiaromaticity. Herein, we investigated the stacked antiaromaticity in the anthracene dimer experimentally and computationally with the aim of elucidating the effect of extension of the π-system from benzene to anthracene.

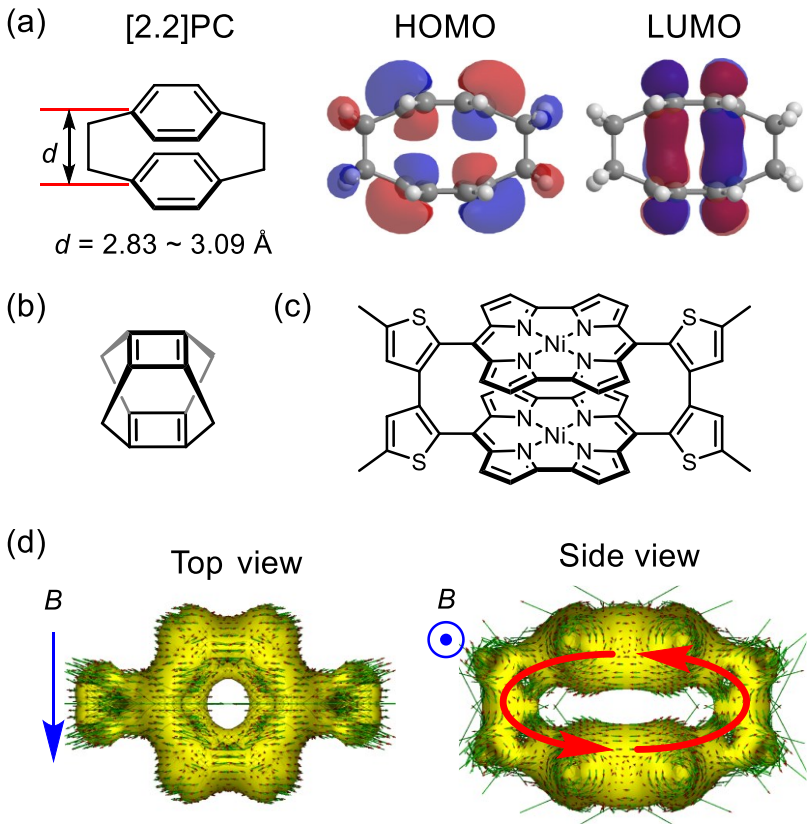


**Figure 1**. (a) The molecular structure of [2.2]PC (left) and its HOMO and LUMO orbitals (right). (b) First proposed a stacked aromatic compound composed of two cyclobutadiene rings. (c) Experimentally achieved the stacked aromatic compound composed of two norcorrole rings. (d) Map of anisotropy of the induced current density (ACID) of [2.2]PC. Top view (left) and side view (right) with applied magnetic field (blue arrows) from top to down and from back to front, respectively. In the side view, paratropic ring current (red arrows) is observed between two benzene rings.

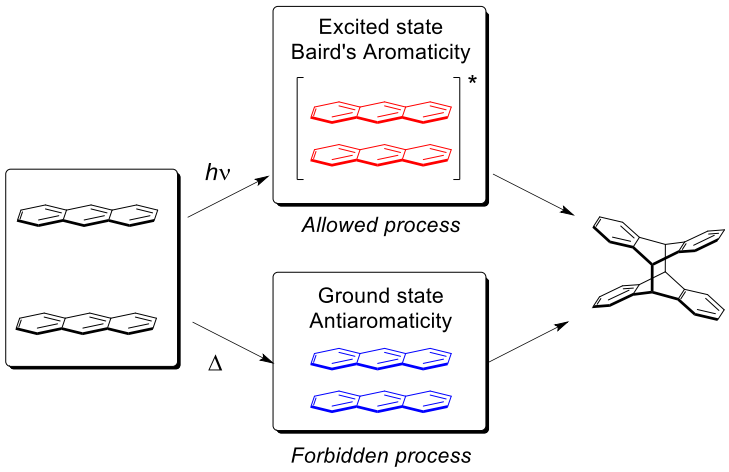


**Figure 2**. Pericyclic [4+4] dimerization of two anthracenes. The excited state excimer has Baird's aromaticity and is the dimerization reaction is an allowed process, while the ground state closely stacked anthracene dimer is antiaromaticity and dimerization is a forbidden process.

## 2. Experimental

### 2.1. Computational methods

All calculations were performed by using the Gaussian 16 program.[12] Geometry optimizations for the anthracene dimers, gauge-including magnetically induced currents (GIMIC) calculations,[13] and NICS calculations[14] were performed using DFT method with long-range-corrected (LRC) functionals CAM-B3LYP[15] adding the D3 version of Grimme's dispersion with the original D3 damping function.[16] The unperturbed and magnetically-perturbed electron densities necessary for GIMIC calculations were obtained at the same level of approximation as those for NICS calculations. The external magnetic field was applied in two directions including parallel (*x*-axis) and perpendicular (*z*-axis) to the molecular plane. The MIC densities were evaluated by using GIMIC version 2.1.4 and Gaussian2gimic.py programs. DrawMol application[17] was used for visualizations of three-dimensional (3D) plots as well as two-dimensional (2D) plots on several cross-sectional surfaces of MIC vector fields. Biradical character of the anthacene dimers were calculated from natural orbital occupation number using broken-symmetry method. TD-DFT calculations of anthracenopahne **1** were performed using CAM-B3LYP functional with a tuned parameter method ($\mu = 0.150$, $\alpha = 0.0799$, $\beta = 0.9201$ [$\alpha + \beta = 1.0$]). [18, 19]

### 2.2. X-ray crystallographic analysis using diamond anvil cell

X-ray crystal analysis under hydrostatic pressure were collected at 296 K on Rigaku XtaLAB Synaergy Custom (Detector is Hypix-6000HE. Mo-Kα (λ = 0.71069 Å)). A sample holder equipped with a DAC (inside diameter 0.35 mm, thickness 0.15 mm, angular aperture 60°) was used for the measurements. The sample was placed in a DAC filled with the pressure medium of methanol/ethanol (4/1 vol%). The inner pressures in the DAC were determined by the unit-cell parameters of NaCl.[20]

## 3. Results and Discussion

### 3.1. Computational studies of the antiaromaticity in benzoannulated anthracenophane **1**

The impetus for this study came from a curious about a broad weak absorption from 450 to 550 nm observed in benzoannulated anthracenophane **1**,[21] having short aromatic C···C distance *ca*. 2.80 Å (Figure 3a-b). Such a broad weak absorption is not observed in acyclic anthracene congested molecules such as 1,2-di(9-anthryl)benzene **2**[22] and 1,2,3-tri(9-anthryl)benzene **3**(Figure 3c).[23] The Kohn-Sham molecular orbitals and TD-DFT calculation reveal that the broad absorption band from 450 to 550 nm observed for **1** corresponds to a HOMO-LUMO transition (536.40 nm, $f$ = 0.0020), through which the molecular orbital distribution mainly locates on the central six-membered ring of the anthracene moiety (Figure S1-S2). By analyzing the HOMO and LUMO orbitals, these bonding orbital distribution manner are identical with those of cyclooctatetraene (COT) with planar $D_{4h}$ symmetry, which is known to show the 8π antiaromaticity (Figure 4).[24] In fact, planar COT derivatives also show the similar broad weak absorption, originating from forbidden HOMO-LUMO transition.

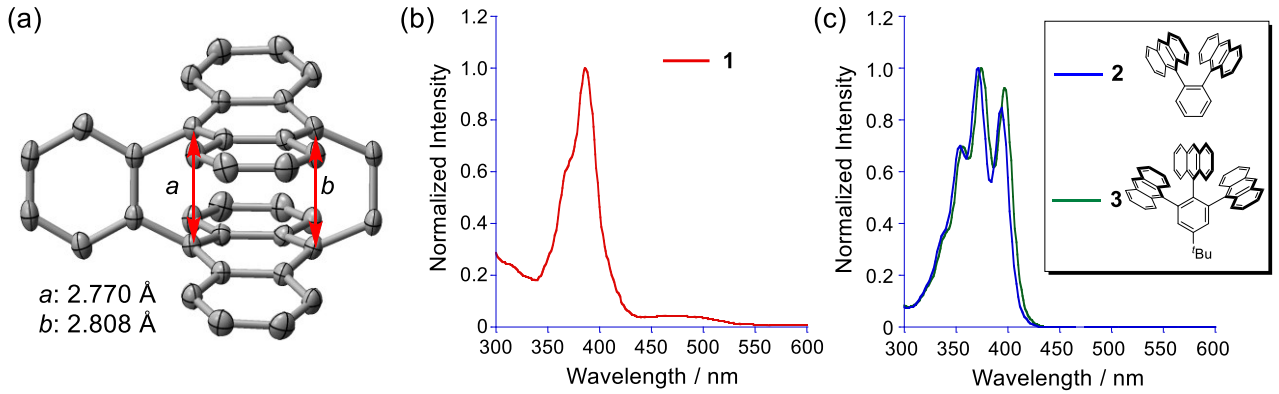


**Figure 3**. (a) X-ray crystallography of benzoannulated anthracenophane **1**.[21] (b) UV-vis absorption of **1**. (c) UV-vis absorption of acyclic reference compounds **2** and **3**.

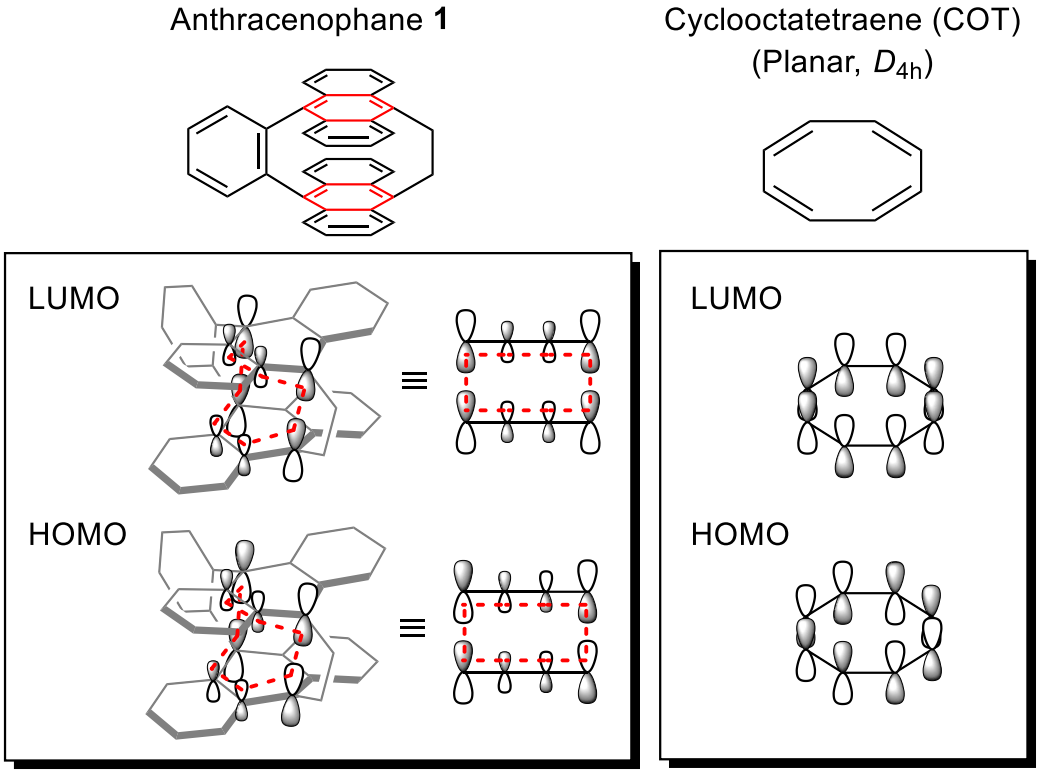


**Figure 4**. Graphic representation of π-molecular orbitals (HOMO and LUMO) of anthracenophane **1**, which extracts central six-membered rings related with 8π-enectrons (left), and planar COT (right). Red dashed lines in π-molecular orbitals of **1** indicate the 8π system, which is the identical orbital distribution manner that of planar COT.

Therefore, to evaluate the 8π antiaromatic system within the two π-congested anthracene units, gauge-including magnetically induced current (GIMIC) calculations were performed. This treatment is a powerful tool used to gain an understanding the aromatic nature of a system in terms of the response of electrons with respect to the external magnetic field. In addition, nucleus-independent chemical shift (NICS) calculations were conducted for **1**, using X-ray crystallographic structure, as well as **1'**, without benzene and ethylene tethers in **1**. The

calculations were conducted by using CAM-B3LYP/6-311+G(d,p) level of theory.[25] The molecular orientation of **1** for the calculations is fixed with the long axis direction of anthracene unit being the *x*-axis, the short axis direction of anthracene unit being the *y*-axis, and the stacking direction of two anthracene units being the *z*-axis (Figure 5a). The magnetically induced current (MIC) density vector plots of **1** applying the magnetic field on *x*-axis is shown in Figures 5b (3D plot) and 5c (2D plot), and in Figure 5d (indicating the sliced plane of 2D plot) is shown the weak paratropic ring current present between two anthracenes thorough ethylene and benzene units (Figure S3). The ring currents indicate an inclusion of σ-conjugation because, in the HOMO−1 and LUMO, σ-bonding orbitals on ethylene and benzene tethers could be confirmed (Figure S1), resulting in [8π+4σ] electron system which is the identical that of [2.2]PC.[8] On the other hand, the neighboring annulated benzene ring shows a strong diatropic ring current toward the magnetic field (See also in Movie S1). Next, MIC density vector plot of **1'** was explored to elucidate the 8π current circuit between the two anthracene moieties (Figure 6 and Figure S4). It is noteworthy that sufficient through-space paratropic ring current exists between the two anthracenes even when the system does not contain ethylene and benzene tethers (Movie S2). However, the vector intensities are relatively weak probably because this is not the through-bond conjugation but the through-space conjugation. Therefore, this is why the σ-conjugation through ethylene and perpendicular benzene tethers in **1** would appear to be more prominent than the through-space π-conjugation between two anthracenes, and these two paratropic ring currents of [8π+4σ] and 8π electron systems are found to be mixed in the anthracenophane **1**.

NICS values ($NICS_{iso}$, $NICS_{xx}$, $NICS_{yy}$, and $NICS_{zz}$) between the space of two anthracenes in **1** and **1'** are calculated and the values at three points, α (the center of central six-membered ring of anthracene unit), β (the center of terminal six-membered ring of anthracene unit), γ (center between α and α'), and δ (center between β and β') are summarized in Table 1 for **1** and Table 2 for **1'**. The $NICS_{iso}$ and $NICS_{zz}$ values of **1** show large negative signs for all four point, indicating these points possess an aromaticity. In particular, γ position, the center of the two anthracenes, shows the largest negative $NICS_{iso}$ (−17.7 ppm) and $NICS_{zz}$ (−58.1 ppm). On the other hand, $NICS_{xx}$ value in γ position for **1** shows a moderate positive sign of +6.53 ppm indicating there is a weak antiaromaticity with *x*-axis direction because the [8π+4σ] and 8π electron system between the two anthracenes is perpendicular to the *x*-axis. Same trend was observed in [2.2]PC that the $NICS_{xx}$ value at the center between two benzene rings is +6.84 ppm (Figure S12). Interestingly, the $NICS_{xx}$ value at γ position of **1'**, without tethers from **1**, shows a greater positive value of +16.7 ppm than that of **1**. Furthermore, the $NICS_{\pi}$ values, from which only the π-electron contribution is extracted, are also examined for **1'** using the canonical molecular orbital (CMO) dissociation method[26] with CAM-B3LYP/6-31+G(d) level of theory[27] (Table 3 and Table S1-S2). At all four points, these $NICS_{\pi xx}$ show relatively large positive values and, in particularly, the $NICS_{\pi xx}$ value at γ position shows +24.1 ppm. In addition, $NICS_{\pi zz}$ values at α and β at which is located on the anthracene shows larger negative values of −44.2 and −34.3 ppm, respectively, from those of $NICS_{zz}$ of −30.7 and −17.2 ppm, while $NICS_{\pi zz}$ values at γ and δ at which is located on the space between anthracenes shows smaller negative values of −46.2 and −26.9 ppm, respectively, from those of $NICS_{zz}$ of −56.8 and −40.3 ppm. These results indicated that the anthracene unit itself in the dimer possesses an aromatic character (Figure S7 and Movie S9), but the space between two anthracene possesses an antiaromatic character toward the *x*-axis direction. However, the antiaromatic character of **1** seems to be weaken by the large aromatic character suffering from the two anthracenes and/or by the existence of σ-conjugation through ethylene and benzene tethers.

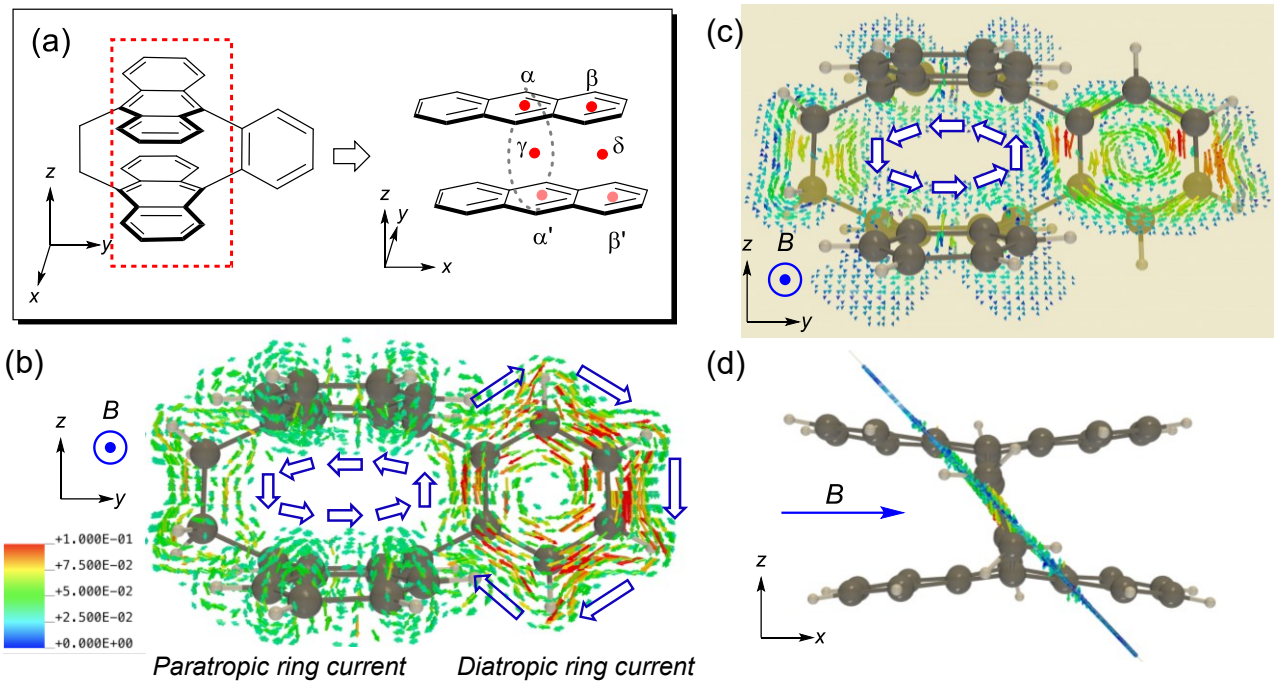


**Figure 5**. (a) Calculated molecular orientation of compound **1**. To clarify the NICS calculation points, two anthracene moiety is highlighted with red dashed square (left) and rotated 90° on the *x*-*y* plane and shown on the right. The benzene and ethylene tethers are omitted by the dashed lines between two anthracenes (right). (b) 3D Magnetically induced current (MIC) density vector plot of **1**. Magnetic field *B* is applied on *x*-axis (from back to front in this figure). The values in the color bar are given in a.u.. The current vectors are scaled with a factor of 5 Å a.u.$^{-1}$, where 1 a.u. = 100.63 nA T$^{-1}$ Å$^{-2}$. The current vectors with amplitudes less than 0.03 a.u. are not illustrated. Big blue arrows between the space of two anthracenes, and peripheral of benzene ring indicate the MIC direction. (c) 2D MIC density vector plot of **1** viewing from *x*-axis. The current vectors with amplitudes less than 0.01 a.u. are not illustrated. (d) Side view of the 2D MIC density vector plot of **1**, indicating the sliced plane, as shown in (c).

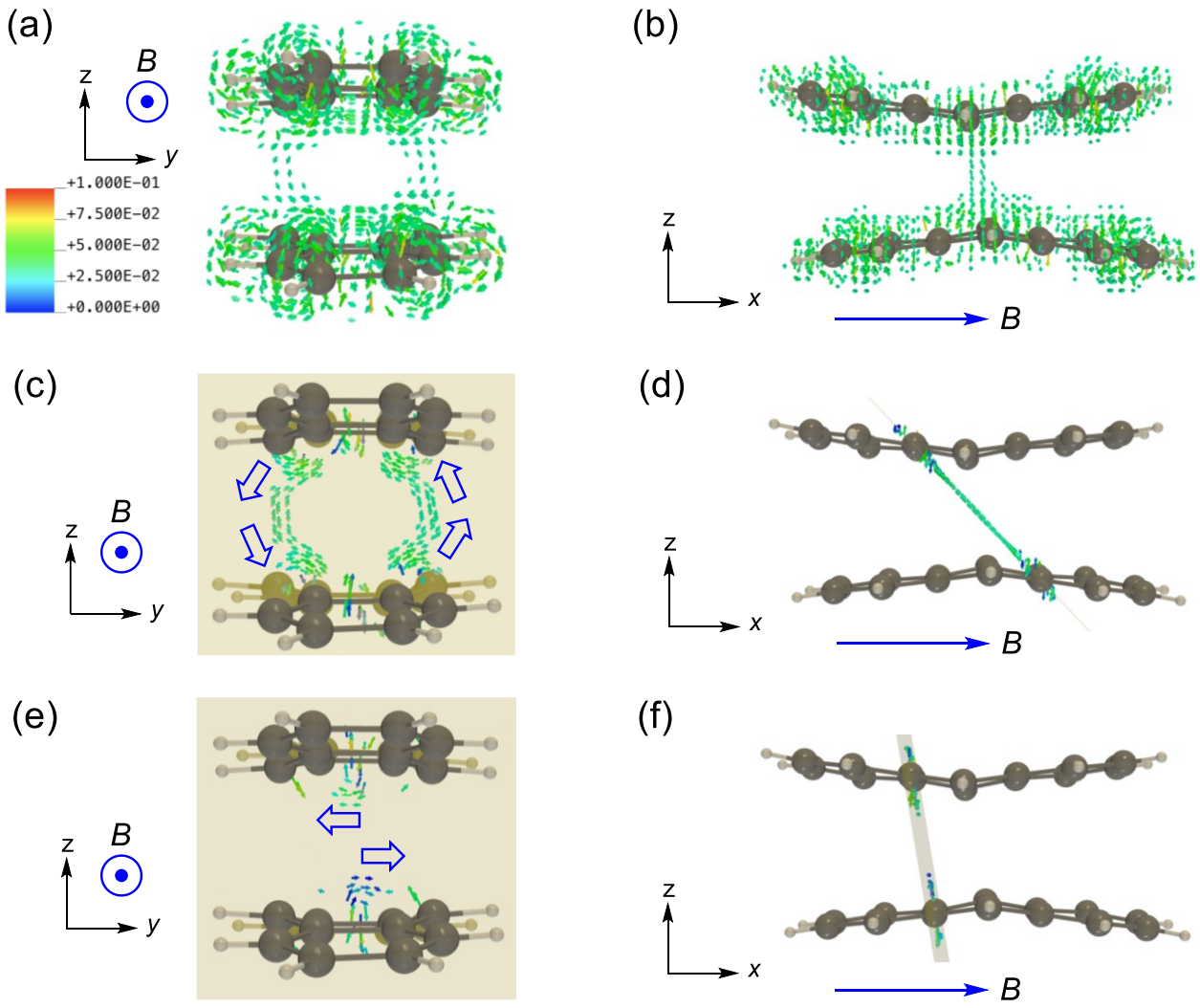


**Figure 6**. (a) 3D MIC density vector plot of **1**' viewing from *x*-axis. Magnetic field *B* is applied on *x*-axis (from back to front in this figure). The values in the color bar are given in a.u.. The current vectors are scaled with a factor of 5 Å a.u.$^{-1}$, where 1 a.u. = 100.63 nA T$^{-1}$ Å$^{-2}$. The current vectors with amplitudes less than 0.03 a.u. are not illustrated. (b) Side view (viewing from *y*-axis) of the 3D MIC density vector plot of **1**'. (c) 2D MIC density vector plot of **1**' viewing from *x*-axis. Large blue arrows between two anthracenes indicate the current direction. The current vectors with amplitudes less than 0.03 a.u. are not illustrated. (d) Side view of the 2D MIC density vector plot of **1**', indicating the sliced plane, as shown in (c). (e) 2D MIC density vector plot of **1**' viewing from *x*-axis. Large blue arrows between two anthracenes indicate the MIC direction. The current vectors with amplitudes less than 0.03 a.u. are not illustrated. (f) Side view of the 2D MIC density vector plot of **1**', indicating the sliced plane, as shown in (e).

**Table 1**. NICS values (ppm) of α, β, γ, and δ positions between two anthracenes in **1**. (CAM-B3LYP/6-311+G(d,p))

| | $NICS_{iso}$ | $NICS_{xx}$ | $NICS_{yy}$ | $NICS_{zz}$ |
|---|---|---|---|---|
| α | –12.2 | –1.02 | –7.17 | –28.3 |
| β | –7.18 | –3.45 | –5.29 | –12.8 |
| γ | –17.7 | +6.53 | –1.50 | –58.1 |
| δ | –11.1 | +3.39 | +2.38 | –39.0 |

**Table 2**. NICS values (ppm) of α, β , and γ positions between two anthracenes in **1'**. (CAM-B3LYP/6-311+G(d,p))

| | $NICS_{iso}$ | $NICS_{xx}$ | $NICS_{yy}$ | $NICS_{zz}$ |
|---|---|---|---|---|
| α | –10.3 | +4.45 | –4.61 | –30.7 |
| β | –7.81 | –0.64 | –5.59 | –17.2 |
| γ | –12.0 | +16.7 | +4.07 | –56.8 |
| δ | –9.77 | +7.13 | +3.85 | –40.3 |

**Table 3**. $NICS_{\pi}$ values (ppm) of α, β , and γ positions between two anthracenes in **1'**. (CAM-B3LYP/6-31+G(d))

| | $NICS_{\pi iso}$ | $NICS_{\pi xx}$ | $NICS_{\pi yy}$ | $NICS_{\pi zz}$ |
|---|---|---|---|---|
| α | –9.84 | +13.6 | +0.97 | –44.2 |
| β | –9.40 | +7.68 | –26.4 | –34.3 |
| γ | –3.36 | +24.1 | +12.1 | –46.2 |
| δ | –1.61 | +14.4 | +7.61 | –26.9 |

3.2. Computational studies of the antiaromaticity in anthracene dimer

To obtain deeper insight, we also calculated anthracene dimer without tethers with $D_{2h}$ symmetry for evaluating the distance dependency of the HOMO-LUMO energies, the paratropic ring current, and NICS values between the π-congested space of two anthracenes. Figure 7a shows the relationship between C9···C9' distances of two anthracenes and its molecular orbital energies of HOMO−1, HOMO, LUMO and LUMO+1 calculated by RCAM-B3LYP-D3/6-31G** level of theory. The structure of anthracene dimers were fixed as $D_{2h}$ symmetry. By shortening the C9···C9' distance from 3.30 Å by 0.1 Å, the HOMO-LUMO gap was found to be decreased dramatically whereas no significant changing were observed in the energies of HOMO−1 and LUMO+1. After showing the minimum HOMO-LUMO gap at 2.40 Å, the HOMO-LUMO gap was found to increase with shortening C9···C9' distance. In addition, the bonding and antibonding manners of HOMO and LUMO orbitals between two anthracenes are reversed at between 2.50 Å and 2.40 Å (Figure 7b). Therefore, these C9···C9' distances should be the transition state of [4+4] cyclization in the ground state. To more elucidate, unrestricted broken-symmetry calculation method with the same level of theory (UCAM-B3LYP-D3/6-31G**) around 2.40 Å of the distance at C9···C9' were also computed.

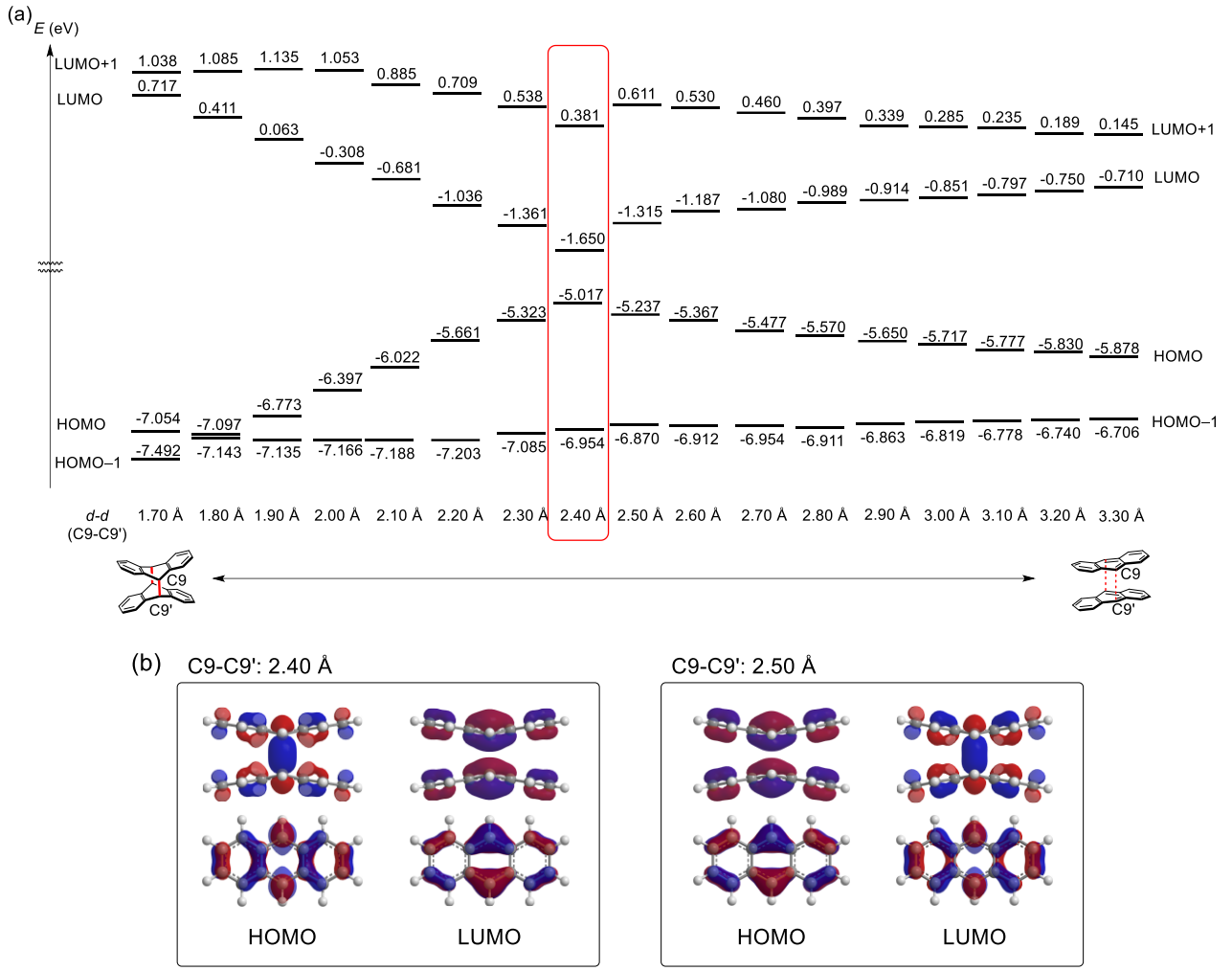


**Figure 7**. (a) Molecular orbital energy diagrams of anthracene dimer with different distances at C9···C9' from 3.30 to 1.70 Å ($D_{2h}$ symmetry) calculated by RCAM-B3LYP/6-31G** level of theory. (b) HOMO and LUMO orbitals of anthracene dimers with C9···C9' distance at 2.40 Å (left) and 2.50 Å (right).

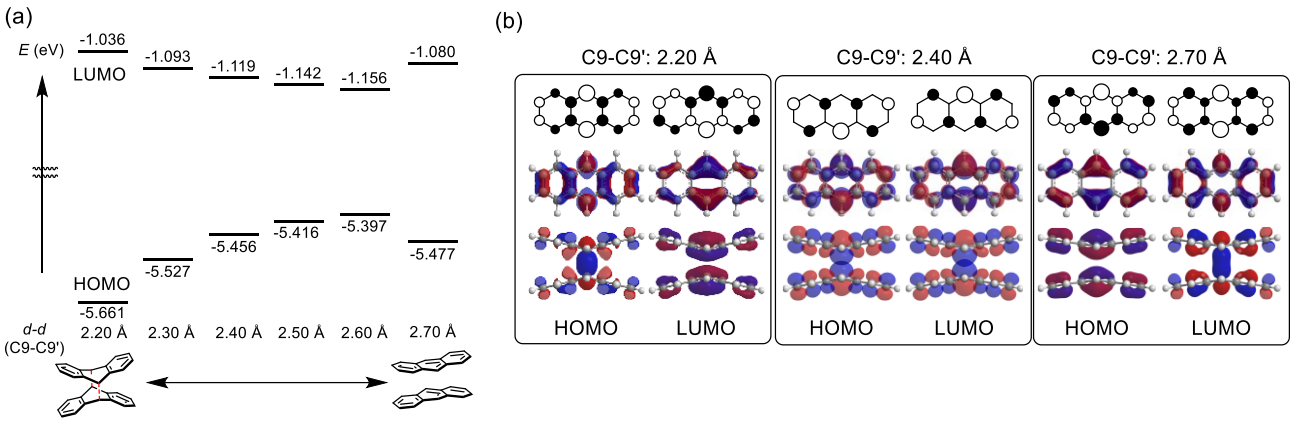


**Figure 8**. (a) Molecular orbital energy diagrams of anthracene dimer with different distances at C9···C9' from 2.70 to 2.20 Å ($D_{2h}$ symmetry) calculated by (U)CAM-B3LYP/6-31G(d,p) level of theory. Open-shell contribution was observed from 2.30 to 2.60 Å whereas closed-shell contribution was observed at 2.20 and 2.70 Å. (b) HOMO and LUMO orbitals of anthracene dimers with C9···C9' distance at 2.20 Å (left), 2.40 Å (center), and 2.70 Å (right).

**Table 4**. Distance dependency of biradical character (%) in anthracene dimer. The biradical character was estimated from natural orbital occupation number (NOON) of LUMO.

| C9···C9' distance (Å) | 2.20 | 2.30 | 2.40 | 2.50 | 2.60 | 2.70 |
|---|---|---|---|---|---|---|
| Biradical character (%) | 0.0 | 56.4 | 88.0 | 42.4 | 6.8 | 0.0 |

The HOMO-LUMO gaps in the unrestricted calculations afforded slightly increased by lowering HOMO and increasing LUMO compared from those in the restricted calculations because there is the contribution of open-shell character (Figure 8a). Thus, the molecular orbital distribution at 2.40 Å possesses a non-bonding pattern in both HOMO and LUMO whereas those at 2.20 Å and 2.70 Å possess bonding and anti-bonding patterns in HOMO and LUMO (Figure 8b). In addition, significant biradical character was observed in the range of 2.30 Å to 2.60 Å and the maximum biradical character 88.0% is confirmed at 2.40 Å (Table 4). Regarding the structure at 2.20 Å of C9···C9' distance, C($sp^3$)-C($sp^3$) single bond formations probably occur even at long carbon-carbon distance judging from the existence of a bonding orbital between C9···C9' position in HOMO and no biradical character at this point.[25] Thus, it can be considered that, for anthracene dimer, the dimer structure in the range of 2.30 Å to 2.60 Å is the transition state of bond order changing between $sp^2$ carbon and $sp^3$ carbon at C9 and C9' positions. In the case of benzene dimer, the generation of biradical character is also observed but the distance between two benzene rings is closer at 2.10 Å with relatively small biradical character of 23.5% (Figure S15-S16), indicating that the π-extension from benzene to anthracene effectively enhances the biradical character with longer distance of two aromatic planes. The distance dependency of the singlet-triplet (S-T) energy gaps for anthracene dimer were also calculated and it is noteworthy that the minimum S-T gap is still 10.5 kcal $mol^{-1}$ even the distance at 2.40 Å having a large biradical character (Figure S17). This large S-T gap is probably because the structure is the transition state to form new C-C bonds and, therefore, singlet state is energetically favorable than that of triplet state.

GIMIC and NICS calculations were conducted using the structure with the C9···C9' distance at 2.40, 2.70, 3.00, and 3.30 Å (The molecular orientation is shown in Figure 9). Different from anthracenophane **1**, MIC plots of the anthracene dimer at 2.40 and 2.70 Å with $D_{2h}$ symmetry show strong through-space conjugation between anthracenes, resulting in the intense paratoropic ring current within the 8π system (Figure 10-11 and Figure S8-S9). On the other hand, when the C9···C9' distance is at 3.00 and 3.30 Å, the paratropic ring currents between the anthracenes are very weak (Figure S10-S11). The NICS calculations at the distance of 2.40 Å showed that large positive sign of *xx* tensor was observed not only at γ (+45.0 ppm) and δ (+15.6 ppm) but also at α (+27.7 ppm) due to the large biradical nature (Table 5). It is noteworthy although the NICS*xx* values at γ position is gradually reduced by the C9···C9' distance elongated, there is still high positive NICS*xx* value of +28.4 ppm at 2.70 Å of the C9···C9' distance, even though the anthracene dimer with the distance is closed-shell species (Table 6 and Table S5). In addition, NICS calculations of anthracene monomer, which is extracted from the structure of anthracene dimers with different C9···C9' distances (2.40, 2.70, 3.00, and 3.30 Å), were also computed to evaluate the loss or gain of (anti)aromaticity on the anthracene unit (Table S6). Compared with the NICS values of anthracene monomer, the anthracene dimer with 2.40 Å showed the loss of aromaticity in $NICS_{iso}$ as well as in $NICS_{zz}$ values except for γ position of $NICS_{zz}$ value. The same tendency was observed for the anthracene dimer with 2.70 Å but the degree of loss of aromaticity decreased. On the contrary, increasing of aromaticity (large negative sign of NICS value) was observed in $NICS_{zz}$ at γ position due to suffering diatropic ring current from two anthracenes.[26] The anthracene dimer with 3.00 and 3.30 Å showed no such a loss of aromaticity and increasing of aromaticity due to the

aforementioned reason.

Therefore, by congesting two anthracenes less than the sum of van der Waals's radii of carbon atoms, the distance of two anthracenes around 2.40 Å affords the biradical nature at where is the transition state of bond order changing between $sp^2$ carbon and $sp^3$ carbon. The most important point is that the system of anthracene dimer starts to develop the paratropic ring current before reaching to the transition state, which is observed in the anthracenophane **1**.

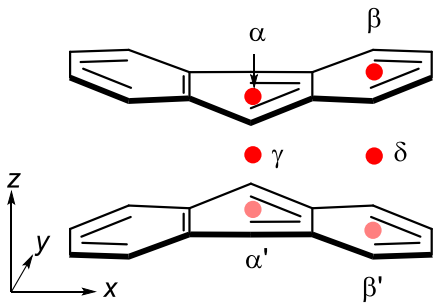


**Figure 9**. Calculated molecular orientation of anthracene dimer (C9···C9': 2.40, 2.70, 3.00, and 3.30 Å). The NICS calculated points, α, β, γ, and δ, are located at the center of central six-membered ring of anthracene, the center of terminal six-membered ring of anthracene, the center of the anthracene dimer (between α and α'), and the center between β and β', respectively.

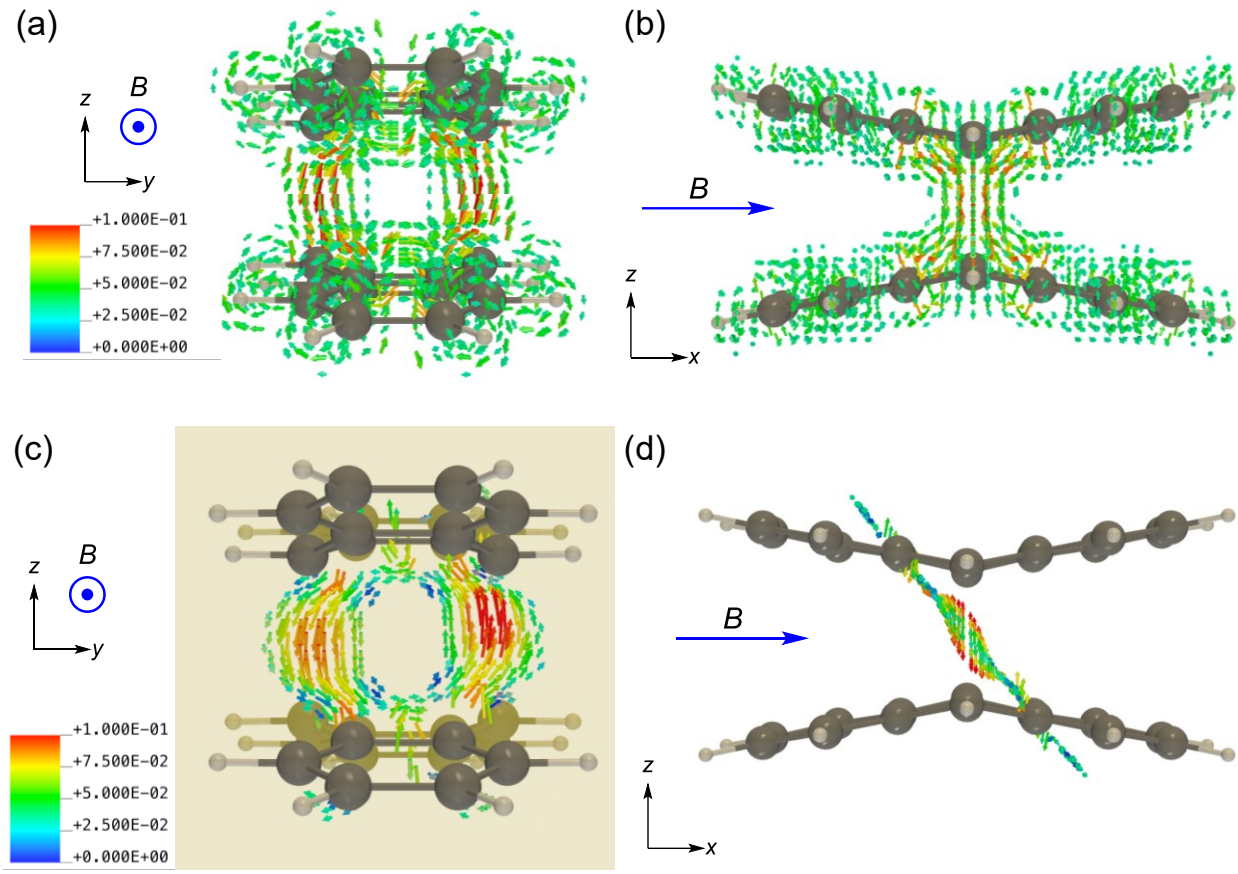


**Figure 10**. (a) 3D MIC plots of the anthracene dimer with the C9···C9' distance at 2.40 Å viewing from *x*-axis. Magnetic field *B* is applied on *x*-axis (from back to front in this figure). The values in the color bar are given in a.u.. The current vectors are scaled with a factor of 5 Å a.u.$^{-1}$, where 1 a.u. = 100.63 nA T$^{-1}$ Å$^{-2}$. The current vectors with amplitudes less than 0.03 a.u. are not illustrated. (b) MIC plots of the anthracene dimer viewing from *y*-axis. (c) 2D MIC density vector plot of the anthracene dimer viewing from *x*-axis. The current vectors with amplitudes less than 0.03 a.u. are not illustrated. (d) Side view of the 2D MIC density vector plot, indicating the sliced plane, as shown in (c).

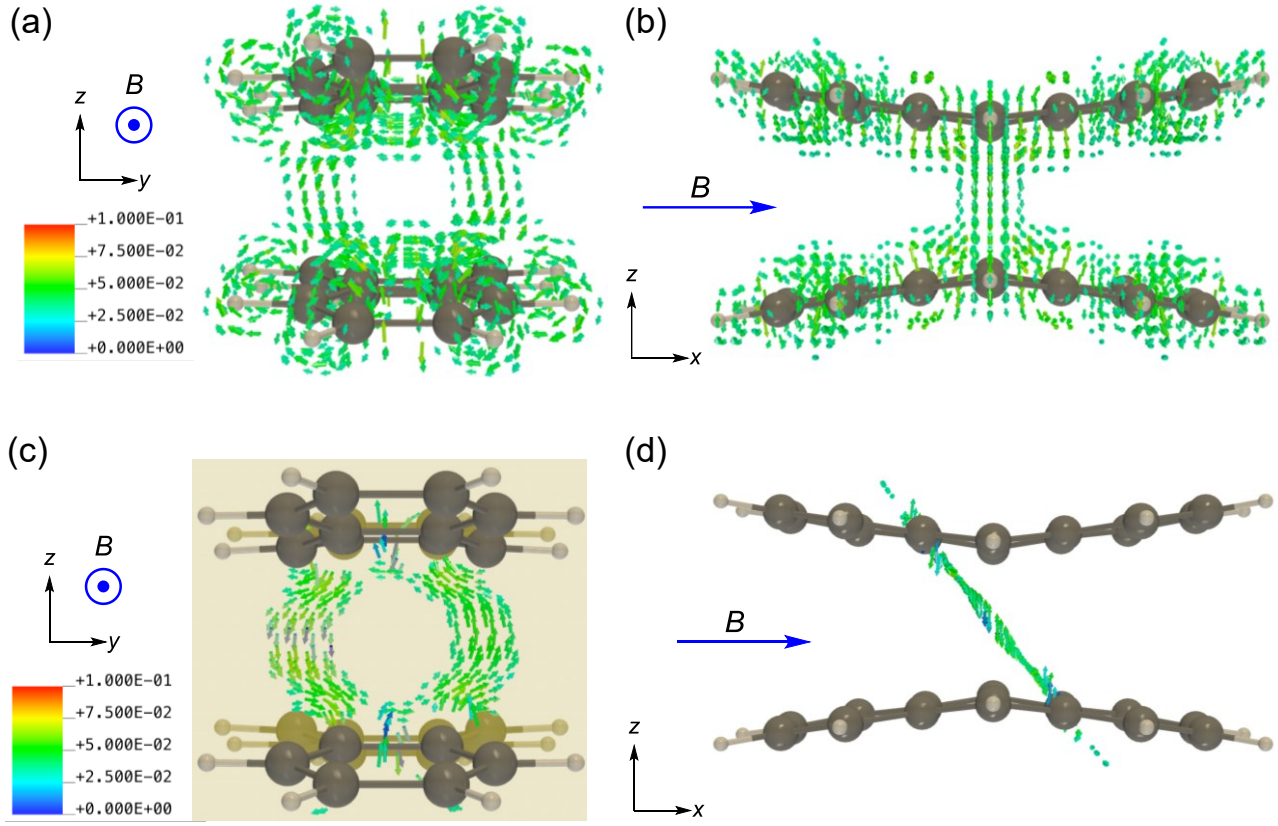


**Figure 11**. (a) 3D MIC plots of the anthracene dimer with the C9···C9' distance at 2.70 Å viewing from *x*-axis. Magnetic field *B* is applied on *x*-axis (from back to front in this figure). The values in the color bar are given in a.u.. The current vectors are scaled with a factor of 5 Å a.u.$^{-1}$, where 1 a.u. = 100.63 nA T$^{-1}$ Å$^{-2}$. The current vectors with amplitudes less than 0.03 a.u. are not illustrated. (b) MIC plots of the anthracene dimer viewing from *y*-axis. (c) 2D MIC density vector plot of the anthracene dimer viewing from *x*-axis. The current vectors with amplitudes less than 0.03 a.u. are not illustrated. (d) Side view of the 2D MIC density vector plot, indicating the sliced plane, as shown in (c).

**Table 5**. NICS values (ppm) of α, β, γ, and δ positions of anthracene dimer (C9···C9': 2.40 Å). Calculated by UCAM-B3LYP/6-311+G(d,p)//UCAM-B3LYP-D3/6-31G(d,p).

| | $NICS_{iso}$ | $NICS_{xx}$ | $NICS_{yy}$ | $NICS_{zz}$ |
|---|---|---|---|---|
| α | +9.28 | +27.7 | –8.35 | +8.45 |
| β | –3.80 | –2.54 | –5.79 | –8.14 |
| γ | +8.36 | +45.0 | –2.15 | –17.7 |
| δ | –5.03 | +15.6 | +1.48 | –32.1 |

**Table 6**. $NICS_{xx}$ values (ppm) of α, β, γ, and δ positions of anthracene dimer with the C9···C9' distance from 2.40, 2.70, 3.00, and 3.30 Å. Calculated by UCAM-B3LYP/6-311+G**//UCAM-B3LYP-D3/6-31G**.

| C9···C9' / Å | α | β | γ | δ |
|---|---|---|---|---|
| 2.40 | +27.7 | –2.54 | +45.0 | +15.6 |
| 2.70 | +12.5 | +1.44 | +28.4 | +12.5 |
| 3.00 | +1.52 | –1.65 | +12.9 | +7.33 |
| 3.30 | –2.35 | –3.13 | +6.90 | +5.02 |

3.3. Attempt to enhance the antiaromaticity of **1** using hydrostatic pressure

Computational studies of the anthracene dimer indicated that the closing distance between two anthracenes gives a large antiaromaticity within the π-congested space as well as a biradical open-shell character. However, the range of distance between two anthracenes at which exhibits the unique properties is 2.30 to 2.50 Å. It seems difficult to reach such a quite short distance between non-covalent carbon-carbon atoms under mild condition. Therefore, we attempted the enhancement of the antiaromaticity of **1** by applying a hydrostatic pressure to the crystal of **1** using diamond anvil cell (DAC). Upon applying the pressure, the color of single crystal **1** gradually turned from red (0 GPa) to dark red (5.0 GPa), that is, piezochromic behavior even though **1** has no flexible π-skeletons which readily reflecting the structural changing by its color.[27-29] (Figure 9a). X-ray crystallography under the high pressure revealed that the C-C distances of C9-C9' and C10-C10' are slightly shortened from 2.777 Å to 2.755 Å and 2.826 Å to 2.788 Å, respectively (Figure 9b). TD-DFT calculations of **1** showed that the longer-wavelength shift of HOMO-LUMO transition by applying pressure from 543 nm ($f$ = 0.0017) to 592 nm ($f$ = 0.0029) was observed (Figure S18). However, NICS values at γ position showed that no enhancement of antiaromaticity by applying pressure at 5.0 GPa was calculated (Table 7, Figure S5, S6, and Table S3). Therefore, unfortunately in this study, it was difficult to reach less than 2.600 Å at which exhibits the biradical character with large antiaromaticity.

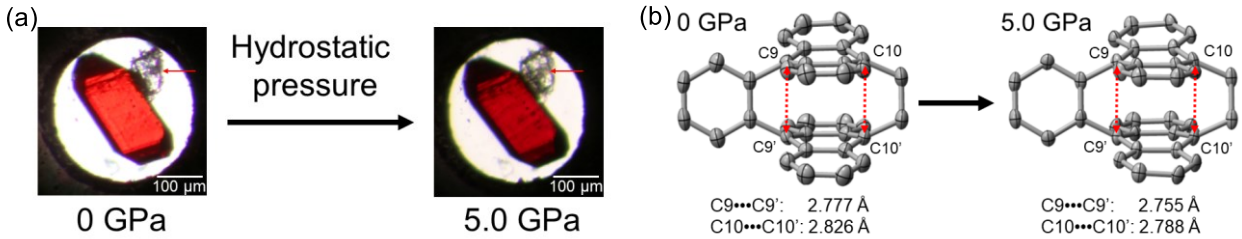


**Figure 12**. (a) Color changing of the single crystal of **1** from red (0 GPa) to dark red (5.0 GPa). Red arrows indicate a NaCl crystal as an internal standard for measurement of the pressure. (b) Structural changing of X-ray structure of **1** before and after applying pressure at room temperature. Red dashed lines indicate the distances between C9 and C9', and C10 and C10'. Hydrogens are omitted for clarity.

**Table 7**. NICS values (ppm) of α, β , and γ positions between two anthracenes in **1** under 5.0 GPa Calculated points (α, β, γ, and δ) are shown in Figure 5a. (CAM-B3LYP/6-311+G(d,p))

| | $NICS_{iso}$ | $NICS_{xx}$ | $NICS_{yy}$ | $NICS_{zz}$ |
|---|---|---|---|---|
| α | –12.3 | –1.33 | –7.37 | –28.2 |
| β | –8.58 | –2.83 | –6.09 | –16.8 |
| γ | –18.5 | +5.18 | –1.33 | –59.5 |
| δ | –12.4 | +2.65 | +2.61 | –42.4 |

## 4. Conclusion

We have computationally revealed that a stacked antiaromaticity within the π-congested space of anthracene dimer is generated because 8π antiaromatic system is formed between the central six-membered rings of anthracenes. In addition, by shortening the C···C distances between two anthracene, not only the enhancement of positive NICS value but also large biradical character about 88% at 2.40 Å were observed, attributing from the transition state of bond order changing between $sp^2$ carbon to $sp^3$ carbon. In the case of benzene dimer, same trends are observed but there are small biradical character about 23.5% with closer distance at 2.10 Å. Thus, this stacked antiaromaticity would be attractive nature to further understand the concept of aromaticity/antiaromaticity and chemical bond, and to explore a functional material which can control the aromaticity and/or antiaromaticity by π-congestion. Unfortunately, it was difficult to enhance the antiaromaticity and to generate the biradical character of anthracenophane **1** by applying the pressure using DAC system. Therefore, the exploring of π-congested stacked molecules with large antiaromaticity and biradical character, realizing under mild condition, is now ongoing.

## Acknowledgement

This study was supported by JSPS KAKENHI JP20K05475 (T.N.), JP21K04995 (R.K.), JP19H00912 (R.K.), and JP22H04974 (R.K.), and by MEXT Grant-in-Aid for Transformative Research Areas (A) JP20H05865 (T.K.) and JP21H05489 (R.K.). The computation was performed using Research Center for Computational Science, Okazaki, Japan (Project: 21-IMS-C152 (T.N.), 22-IMS-C208 (T.N.), and 22-IMS-C004 (R.K.)).

## Conflict of Interest

There are no conflicts of interest to declare.

## ORCID

Tomohiko Nishiuchi: https://orcid.org/0000-0002-2113-0731

Ryohei Kishi: https://orcid.org/0000-0002-6005-7629

Takashi Kubo: https://orcid.org/0000-0001-6809-7396

**Reference**


[1] Selected papers for experimental studies of [2.2]PC, see. a) C. J. Brown, A. C. Farthing, *Nature* **1949**, *164*, 915.; b) D. J. Cram, H. Steinberg, *J. Am. Chem. Soc.* **1951**, *73*, 5691.; c) D. J. Cram, J. M. Cram, *Acc. Chem. Res.* **1971**, *4*, 204.

[2] Selected papers for computational studies of [2.2]PC, see. a) G. F. Caramori, S. E. Galembeck, K. K. Laali, *J. Org. Chem.* **2005**, *70*, 3242.; b) J. Poater, J. M. Bofill, P. Alemany, M. Solà, *J. Org. Chem.* **2006**, *71*, 1700.

[3] a) F. Diederich, *Cyclophanes*. The Royal Society of Chemistry, 1991.; b) J. H. Golden, *J. Chem. Soc.* **1961**, 3741.; c) T. Umemoto, S. Satani, Y. Sakata, S. Misumi, *Tetrahedron Lett.* **1975**, *16*, 3159.; d) R. H. Mitchell, R. J. Carruthers, J. C. M. Zwinkels, *Tetrahedron Lett*. **1976**, *17*, 2585.; e) H. Irngartinger, R. G. H. Kirrstetter, C. Krieger, H, Rodewald. H. A. Staab, *Tetrahedron Lett.* **1977**, *18*, 1425.; f) T. Tsuji, M. Ohkita, J. Nishida, *J. Am. Chem. Soc*. **1993**, *115*, 5284.; g) M. Shibahara, M. Watanabe, T. Iwanaga, T. Matsumoto, K. Ideta, T. Shinmyozu, *J. Org. Chem.* **2008**, *73*, 4433.; h) Y. Morisaki, Y. Chujo, *Polym. Chem.* **2011**, *2,* 1249.; i) F. Schlütter, T. Nishiuchi, V. Enkelmann, K. Müllen, *Polym. Chem*. **2013**, *4*, 2963.

[4] C. Corminboeuf, P. v. R. Schleyer, P. Warner, *Org. Lett.* **2007***, 9*, 3263.

[5] For the concept of stacked aromaticity by congesting two antiaromatic rings, see; a) M. C. Böhm, P. Bickert, K. Hafner, V. Boekelheide, *Proc. Natl. Acad. Sci.* **1984**, *81*, 2589.; b) D. E. Bean, P. W. Fowler, *Org. Lett.* **2008**, *10*, 5573.; c) J-i, Aihara, *J. Phys. Chem. A*. **2009**, *113*, 7945.

[6] a) R. Nozawa, H. Tanaka, W.-Y. Cha, Y. Hong, I. Hisaki, S. Shimizu, J.-Y. Shin, T. Kowalczyk, S. Irle, D. Kim, H. Shinokubo, *Nat. Commun*, **2016**, *7*, 13620.; b) R. Nozawa, J. Kim, J. Oh, A. Lamping, Y. Wang, S. Shimizu, I. Hisaki, T. Kowalczyk, H. Fliegl, D. Kim, H. Shinokubo, *Nat. Commun*, **2019**, *10*, 3576.

[7] R. Herges, D. Geuenich, *J. Phys. Chem. A.* **2001**, *105*, 3214.

[8] D. Geuenich, K. Hess, R. Herges, *Chem. Rev.* **2005**, *105*, 3758.

[9] a) H. E. Zimmerman, *Acc. Chem. Res*. **1971**, *4*, 272.; b) M. J. S. Dewar, *Angew. Chem. Int. Ed. Engl*. **1971**, *10*, 761.

[10] For the concept of Baird's aromaticity, see; a) N. C. Baird, *J. Am. Chem. Soc*. **1972**, *94*, 4941.; b) M. Rosenberg, C. Dahlstrand, K. Kliså, H. Ottoson, *Chem. Rev.* **2014**, *114*, 5379.

[11] V. Vijay, M. Madhu, R. Ramakrishnan, A. Benny, M. Hariharan, *Chem. Commun.* **2020**, *56*, 225.

[12] M. Frisch, G. Trucks, H. Schlegel, G. Scuseria, M. Robb, J. Cheeseman, G. Scalmani, V. Barone, G. Petersson, H. Nakatsuji, X. Li, M. Caricato, A. Marenich, J. Bloino, B. Janesko, R. Gomperts, B. Mennucci, H. Hratchian, J. Ortiz, A.Izmaylov, J. Sonnenberg, D. Williams-Young, F. Ding, F. Lipparini, F. Egidi, J. Goings, B. Peng, A. Petrone, T. Henderson, D. Ranasinghe, V. Zakrzewski, J. Gao, N. Rega, G. Zheng, W. Liang, M. Hada, M. Ehara, K. Toyota, R. Fukuda, J. Hasegawa, M. Ishida, T. Nakajima, Y. Honda, O. Kitao, H. Nakai, T. Vreven, K. Throssell, J. Montgomery, J. Peralta, F. Ogliaro, M. Bearpark, J. Heyd, E. Brothers, K. Kudin, V. Staroverov, T. Keith, R. Kobayashi, J. Normand, K. Raghavachari, A. Rendell, J. Burant, S. Iyengar, J. Tomasi, M. Cossi, J. Millam, M. Klene, C. Adamo, R. Cammi, J. Ochterski, R. Martin, K. Morokuma, O. Farkas, J. Foresman, D. Fox, Gaussian 16, Revision A. 03, Gaussian, Inc., Wallingford, CT2016.

[13] a) J. Jusélius, D. Sundholm, J. Gauss, *J. Chem. Phys.* **2004**, *121*, 3952.; b) S. Taubert, D. Sundholm, J. Jusélius, *J. Chem. Phys.* **2011**, *134*, 54123.; c) H. Fliegl, S. Taubert, O. Lehtonen, D. Sundholm, *Phys. Chem. Chem. Phys.* **2011**, *13*, 20500.; d) M. Rauhalahti, S. Taubert, D. Sundholm, V. Liégeois, *Phys. Chem. Chem. Phys.* **2017**, *19*, 7124.

[14] P. v. R. Schleyer, C. Maerker, A. Dransfeld, H. Jiao, N. J. R. van Eikema Hommes, *J. Am. Chem. Soc.* **1996**, *118*, 6317.

[15] T. Yanai, D.P. Tew, N.C. Handy, *Chem. Phys. Lett.* **2004**, *393*, 51.

[16] S. Grimme, S. Ehrlich, L. Goerigk, *J. Comp. Chem*. **2011**, *32*, 1456.

[17] V. Liegeois, DrawMol ver. 1.6 www.unamur.be/drawmol.

[18] K. Okuno, Y. Shigeta, R. Kishi, M. Nakano, *Chem. Phys. Lett.* **2013**, *585*, 201.

[19] T. Nishiuchi, H. Sotome, R. Fukuuchi, K. Kamada, H. Miyasaka, T. Kubo, *Aggregate* **2021**, *2*, e126.

[20] D. L. Decker, *J. Appl. Phys.* **1971**, *42*, 3239.

[21] T. Nishiuchi, K. Kisaka, T. Kubo, *Angew. Chem. Int. Ed*. **2021**, *60*, 5400.

[22] T. Nishiuchi, S. Uno, Y. Hirao, T. Kubo, *J. Org. Chem.* **2016**, *81*, 2106.

[23] T. Nishiuchi, H. Sotome, K. Shimizu, H. Miyasaka, T. Kubo, *Chem. Eur. J.* **2022**, *28*, e202104245.

[24] Typical examples for planar antiaromatic COTs, see; a) F. W. B. Einstein, A. C. Willis, *J. Chem. Soc. Chem. Commun.* **1981**, 526.; b) F. –G. Klärner, *Angew. Chem. Int. Ed*. **2001**, *40*, 3977.; c) A. Matsuura, K. Komatsu, *J. Am. Chem. Soc.* **2001**, *123*, 1768. d) P. W. Fowler, R. W. A. Havenith, L. W. Jenneskens, A. Soncini, E. Steiner, *Angew. Chem. Int. Ed*. **2002**, *41*, 1558.; e) Y. Nakamura, N. Aratani, H. Shinokubo, A. Takagi, T. Kawai, T. Matsumoto, Z. S. Yoon, D. Y. Kim, T. K. Ahn, D. Kim, A. Muranaka, N. Kobayashi, A. Osuka, *J. Am. Chem. Soc.* **2006**, *128*, 4119.; f) T. Nishinaga, T. Uno, R. Inoue, A. Matsuura, N. Treitel, M. Rabinoviz, K. Komatsu, *Chem. Eur. J.* **2008**, *14*, 2067.; g) T. Ohmae, T. Nishinaga, M. Wu, M. Iyoda, *J. Am. Chem. Soc.* **2010**, *132*, 1066.; h) K. Aita, T. Ohmae, M. Takase, K. Nomura, H. Kimura, T. Nishinaga, *Org. Lett.* **2013**, *15*, 3522.

[25] Because the π-congested circumstance of anthracenophane **1** and anthracene dimers are not a normal molecular structure, we employed CAM-B3LYP functional to avoid an overestimation of the aromaticity and antiaromaticity, see; a) D. W. Szczepanik, M. Solà, M. Andrzejak, B. Pawełek, J. Dominikowska, M. Kukułka, K. Dyduch, T. M. Krygowski, H. Szatylowicz. *J. Comput. Chem*. **2017**, *38*, 1640.; b) I. Casademont-Reig, R. Guerrero-Avilés, E. Ramos-Cordoba, M. Torrent-Sucarrat, E. Matito, *Angew. Chem. Int. Ed*. **2021**, *60*, 24080.

[26] H. Fallah-Bagher-Shaidaei, C. S. Wannere, C. Corminboeuf, R. Puchta, P. v. R. Schleyer, *Org. Lett.* **2006**, *8*, 863.

[27] The CMO dissected NICSπ calculation using CAM-B3LYP/6-311G+(d,p) level of theory resulted in an error because the memory required for NBO calculation could not be allocated.

[25] The spin-spin interaction between the two 9-fluorenyl radicals results in the formation of a closed-shell singlet even when the distance between the two spin centers is 2.04 Å., see; T. Kubo, Y. Suga, D. Hashizume, H. Suzuki, T. Miyamoto, H. Okamoto, R. Kishi, M. Nakano, *J. Am. Chem. Soc.* **2021**, *143*, 14360.

[26] The identical phenomenon that the increasing of aromaticity within the cage of two aromatic planes was already reported. See reference [4], [5b], and [5c].

[27] a) T. Nishiuchi, Y. Kuwatani, T. Nishinaga, M. Iyoda, *Chem. Eur. J.* **2009**, *15*, 6838.; b) T. Nishiuchi, K. Tanaka, Y. Kuwatani, J. Sung, T. Nishinaga, D. Kim, M. Iyoda, *Chem. Eur. J.* **2013**, *19*, 4110.; c) T. Nishiuchi, M. Iyoda, *Bull. Chem. Soc. Jpn.* **2014**, *87*, 960.; d) T. Nishiuchi, M. Iyoda, *Chem. Rec*. **2015**, *15*, 329.

[28] a) C. Yuan, S. Saito, C. Camacho, S. Irle, I. Hisaki, S. Yamaguchi, *J. Am. Chem. Soc.* **2013**, *135*, 8842.; b) K. Nagura, S. Saito, H. Yusa, H. Yamawaki, H. Fujihisa, H. Sato, Y. Shimoikeda, S. Yamaguchi, *J. Am. Chem. Soc.* **2013**, *135*, 10322.; c) C. Yuan, S. Saito, C. Camacho, T. Kowalczyk, S. Irle, S. Yamaguchi, *Chem. Eur. J.* **2014**, *20*, 2193.; d) S. Saito, S. Nobusue, E. Tsuzaka, C. Yuan, C. Mori, M. Hara, T. Seki, C. Camacho, S.

Irle, S. Yamaguchi, *Nat. Commun.* **2016**, *7*, 12094.; e) T. Yamakado, K. Otsubo, A. Osuka, S. Saito, *J. Am. Chem. Soc.* **2018**, *140*, 6245.

[29] a) T. Nishiuchi, S. Aibara, T. Yamakado, R. Kimura, S. Saito, H. Sato, T. Kubo, *Chem. Eur. J.* **2022**, *28*, e202200286.; b) T. Nishiuchi, S. Aibara, H. Sato, T. Kubo, *J. Am. Chem. Soc.* **2022**, *144*, 7479.